J Biomol NMR (2009) 45:143–155
DOI 10.1007/s10858-009-9343-x

ARTICLE

RNA phosphodiester backbone dynamics of a perdeuterated cUUCGg tetraloop RNA from phosphorus-31 NMR relaxation analysis

Jörg Rinnenthal · Christian Richter · Senada Nozinovic · Boris Fürtig · Jakob J. Lopez · Clemens Glaubitz · Harald Schwalbe

Received: 28 May 2009 / Accepted: 19 June 2009 / Published online: 28 July 2009

Abstract We have analyzed the relaxation properties of all ^{31}P nuclei in an RNA cUUCGg tetraloop model hairpin at proton magnetic field strengths of 300, 600 and 900 MHz in solution. Significant H, P dipolar contributions to R_1 and R_2 relaxation are observed in a protonated RNA sample at 600 MHz. These contributions can be suppressed using a perdeuterated RNA sample. In order to interpret the ^{31}P relaxation data (R_1, R_2), we measured the ^{31}P chemical shift anisotropy (CSA) by solid-state NMR spectroscopy under various salt and hydration conditions. A value of 178.5 ppm for the ^{31}P CSA in the static state ($S^2 = 1$) could be determined. In order to obtain information about fast time scale dynamics we performed a modelfree analysis on the basis of our relaxation data. The results show that subnanosecond dynamics detected around the phosphodiester backbone are more pronounced than the dynamics detected for the ribofuranosyl and nucleobase moieties of the individual nucleotides (Duchardt and Schwalbe, J Biomol NMR 32:295–308, 2005; Ferner et al., Nucleic Acids Res 36:1928–1940, 2008). Furthermore, the dynamics of the individual phosphate groups seem to be correlated to the 5′ neighbouring nucleobases.

Keywords NMR spectroscopy · Isotope labeled RNA · ^{31}P relaxation · Modelfree order parameter

Introduction

Many of ribonucleic acids (RNA) functions are related to a multitude of RNA's functional dynamics (Hashim 2007; Al-Hashimi and Walter 2008). Bistable RNA for instance can adopt different conformations of almost equal stabilities (Hobartner and Micura 2003; Hobartner et al. 2004; Wenter et al. 2005, 2006a, b; Fürtig et al. 2007a, b) whereas riboswitch-RNA involved in transcriptional and translational regulation undergo local as well as long-range conformational dynamics upon metabolite binding (Tucker and Breaker 2005; Winkler 2005; Lang et al. 2007; Rieder et al. 2007; Schwalbe et al. 2007). RNA thermometers melt local structure at ambient temperature and thereby regulate translation (Chowdhury et al. 2006; Narberhaus et al. 2006; Waldminghaus et al. 2007). Upon binding to different ligands, TAR–RNA, a potential pharmacological target RNA, can adopt different conformations, many if not all of which are sampled in the free state of the RNA (Zhang et al. 2006, 2007; Ferner et al. 2009).

RNA dynamics span a broad range of time scales from picoseconds where vibrations and angular fluctuations occur up to seconds where catalytic function and global refolding take place (Fürtig et al. 2007a, b). Molecular dynamics (MD) simulations provide a microscopic description of the dynamic trajectories (Miller and Kollman 1997; Williams and Hall 1999, 2000; Nina and Simonson 2002; Showalter et al. 2005; Villa and Stock 2006).

Electronic supplementary material The online version of this article (doi:10.1007/s10858-009-9343-x) contains supplementary material, which is available to authorized users.

J. Rinnenthal · C. Richter · S. Nozinovic · B. Fürtig · H. Schwalbe (✉)
Institute for Organic Chemistry and Chemical Biology, Center for Biomolecular Magnetic Resonance, Johann Wolfgang Goethe-University, Max-von-Laue-Strasse 7, 60438 Frankfurt/Main, Germany
e-mail: schwalbe@nmr.uni-frankfurt.de

J. J. Lopez · C. Glaubitz
Institute for Biophysical Chemistry, Center for Biomolecular Magnetic Resonance, Johann Wolfgang Goethe-University, Max-von-Laue-Strasse 7, 60438 Frankfurt/Main, Germany

NMR spectroscopy can characterize dynamics faster than the overall rotational correlation in the low nanosecond regime from heteronuclear relaxation measurements (R_1, R_2, $R_{1\rho}$, and steady-state heteronuclear NOE) while supra-τ_c motions can be detected from RDC measurements. Subnanosecond dynamics detected in NMR experiments and interpreted in the context of the so-called modelfree formalism can be compared to order parameters predicted from long MD simulations (Koplin et al. 2005; Duchardt et al. 2008; Ferner et al. 2008). If these Lipari-Szabo order parameters S^2_{LS} are known it becomes possible to dissect subnanosecond dynamics from supra-τ_c motions derived from RDC measurements and interpreted by introduction of a so-called RDC order parameter S^2_{RDC}.

Various methods to determine the dynamic properties of RNA have been developed so far. Techniques to determine ^{13}C relaxation in small uniformly ^{13}C-labeled RNAs (Duchardt and Schwalbe 2005; Shajani and Varani 2005, 2007; Shajani et al. 2007; Ferner et al. 2008) and in large specifically ^{13}C-labeled RNAs (Johnson et al. 2006; Johnson and Hoogstraten 2008) as well as ^{13}C relaxation dispersion methods are currently available (Hoogstraten et al. 2000; Blad et al. 2005; Shajani and Varani 2005; Oberstrass et al. 2008; Hansen et al. 2009). Measurement of relaxation properties on samples with selective labeling of specific ^{13}C sites (Olsen et al. 1982; Schmidt et al. 1983, 1987; Williamson and Boxer 1989a, b; Gaudin et al. 1995), uniform partial ^{13}C enrichment (Kojima et al. 1998; Boisbouvier et al. 1999) or at ^{13}C natural abundance (Lane et al. 1991; Borer et al. 1994; Spielmann 1998) have been performed in order to investigate RNA dynamics of the nucleobase and the ribose moieties. ^{15}N relaxation in uniformly ^{15}N-labeled RNA has been measured using methods previously applied in the protein NMR spectroscopy (Akke et al. 1997). Measurements of ^{15}N relaxation properties, however, are restricted to studies of imino resonances involved in hydrogen bonding, since exchange with solvent water is too rapid for conformationally non-stable parts of the RNA.

Measurement of ^{31}P relaxation rates in RNA provides a direct reporter of conformational dynamics of the phosphodiester backbone. Such studies have been performed previously for the sum of all ^{31}P nuclei within RNA constituted in whole virus particles (Kan et al. 1987; Magusin and Hemminga 1994) or ribosomes (Odahara et al. 1994). In this contribution, we provide for the first time a site-resolved investigation of the phosphodiester backbone ^{31}P relaxation properties of a 14mer hairpin RNA. We investigated the cUUCGg tetraloop RNA which constitutes a highly abundant structural RNA motif of extraordinary stability [$T_m \sim 70$°C, (Allain and Varani 1995)]. The cUUCGg motif has been extensively studied and characterized structurally both by NMR spectroscopy (Varani and Tinoco 1991; Allain and Varani 1995; Lynch and Puglisi 2001) and X-ray crystallography (Ennifar et al. 2000).

A number of relaxation studies have been reported for the UUCG tetraloop motif so far. Akke et al. (1997) analyzed the fast time scale motion on the imino resonances of the cUUCGg tetraloop 14mer RNA at 273 K. An S^2 order parameter of 0.75–0.8 was extracted from the ^{15}N relaxation data for all of the ^{1}H–^{15}N bond vectors in stable hydrogen bonds. A model free analysis was also performed on the basis of ^{13}C relaxation data for the aromatic C6H6/C8H8 bond vectors as probes for the nucleobases and the C1′H1′ bond vectors as probes for the ribose moieties (Duchardt and Schwalbe 2005; Ferner et al. 2009). S^2 order parameters between 0.87 and 0.99 were extracted for the nucleobases in the A-form helical part of the RNA at a temperature of 298 K. C1′H1′ bond vectors are well defined with S^2 order parameters between 0.90 and 0.94 in the stem while the loop moieties as well as the ribose moieties of G1 and C14 are slightly more flexible with S^2 values between 0.84 and 0.89. In the UUCG tetraloop, U7 ($S^2 = 0.68$) is more flexible than the rest of the nucleobases. These findings could be reproduced by MD simulations of the cUUCGg tetraloop RNA (Ferner et al. 2008; Villa et al. 2008). Shajani et al. performed ^{13}C relaxation studies for the C5/C6/C8 and the C1′ nuclei on a different RNA bearing a cUUCGg tetraloop (Shajani and Varani 2005). Using an isotropic model for the overall tumbling, S^2 order parameters around 0.9 were obtained for the ribose moieties at a temperature of 298 K. The nucleobases in A-form helical parts of the RNA show S^2 order parameters of around 0.9. For the loop nucleobases varying flexibilities with S^2 values of 0.66–1.0 were reported. In a second study, S^2 order parameters were extracted using different ^{13}C CSA values extracted from liquid crystal measurements (Shajani and Varani 2007). These S^2 order parameters lie between 0.94 (first loop uracil nucleobase) and 0.73 (second loop uracil nucleobase) and are very similar to the S^2 order parameters reported by Ferner et al. (2008). Hall and coworkers analyzed the effects of 2′ ribose substitutions on the thermodynamic stability of UUCG tetraloops by experimental (UV melting curves) and computational methods (Williams and Hall 1999, 2000; Williams et al. 2001) showing the important role of the 2′ hydroxyl group of the first loop uridine on the thermodynamic stability of the UUCG tetraloop.

One obstacle for the interpretation of ^{31}P R_1 and R_2 relaxation rates is the fact that in protonated RNA samples, every phosphorous atom experiences a dipolar field of protons three or four freely rotatable bonds apart, which makes the dipolar contribution to the relaxation dependent on the phosphodiester backbone conformation. We circumvented the problem of quantifying the dipolar relaxation contributions by the use of a perdeuterated RNA

sample for our measurements. Furthermore, the size and orientation of the ^{31}P CSA tensor without dynamic contributions is still not absolutely known. Therefore, we performed solid-state NMR measurements under various salt and hydration conditions to derive the three principal axis components of the CSA tensor in the static state. Using the valid CSA value, we performed a modelfree analysis of our ^{31}P relaxation data in order to obtain site specific information about fast time scale dynamics of the phosphodiester backbone of the 14mer hairpin RNA.

Methods

Sample preparation

Liquid-state NMR measurements were performed using a uniformly ^{2}H-labeled 14mer cUUCGg tetraloop RNA sample with the sequence 5′-PO_4^{2-}–PO_3^{-}–PO_3^{-}GGC AC(UUCG)GUGCC-OH-3′. The sample was purchased from Silantes GmbH (Munich, Germany). The secondary structure of the molecule is shown in Fig. 1a. The RNA was desalted using Vivaspin 20 concentrators with a molecular weight cutoff (MWCO) of 3,000 Da from Sartorius stedim biotech (Aubagne Cedex, France). Refolding of the RNA was achieved by denaturing for 10 min at a concentration of 0.25 mM and a temperature of 95°C followed by 20-fold dilution with ice cold water and subsequent incubation at 0°C for another 30 min. The RNA was concentrated and exchanged to NMR buffer using Vivaspin 20 concentrators (MWCO = 3,000 Da). The correct folding of the RNA was verified by native polyacrylamide gel electrophoresis. The final NMR sample contained 0.8 mM RNA, 20 mM $K_xH_yPO_4$ (pH 6.4 in H_2O), 50 mM KCl, 0.4 mM EDTA and 99.99% D_2O. A ^{13}C, ^{15}N-labeled 14mer cUUCGg RNA tetraloop sample was used for the resonance assignments of the ^{31}P nuclei at 37°C. The sample was prepared in the same way as the ^{2}H-labeled sample.

Solid-state NMR measurements were performed using an unlabeled chemically synthesized 20mer RNA with the sequence 5′-OH-GCGCGCGCGCGCGCGCGCGC-OH-3′. The RNA was purchased from Dharmacon (Boulder, CO). The RNA was deprotected and freeze-dried following the protocol provided by the manufacturers. Subsequently, the RNA was dissolved in water and precipitated at −20°C overnight using 5 volumes of 2% $LiClO_4$ in acetone. The precipitate was dissolved in water. Refolding of the RNA into the duplex conformation was achieved by denaturing for 20 min at a concentration of 1 mM at 95°C followed by slow cooling to room temperature within 30 min. Buffer exchange was achieved using Vivaspin 20 concentrators (MWCO = 3,000 Da). The correct folding of the RNA was verified by native polyacrylamide gel electrophoresis. RNA samples measured in frozen buffer were frozen directly in the NMR spectrometer, while RNA samples measured as a freeze-dried powder were exchanged to the appropriate buffer solution, frozen with liquid nitrogen and freeze-dried. One of the freeze-dried samples was equilibrated to 84% air humidity in an exsiccator within 4 days using a buffer reservoir filled with a saturated KCl/H_2O solution. All NMR sample buffers contained 10 mM MES, pH 6.5 but different KCl concentrations between 0 and 1,000 mM, respectively.

Native gel electrophoresis

5× loading buffer was composed of 87% glycerol, 0.1% (w/v) xylene cyanole FF and 0.1% (w/v) bromophenol

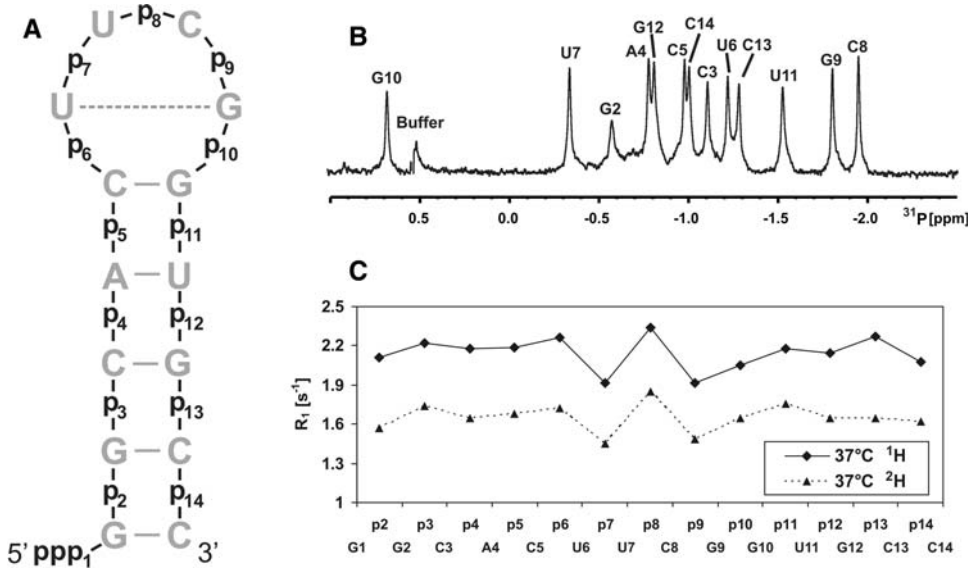

Fig. 1 **a** Secondary structure of the cUUCGg tetraloop 14mer RNA. **b** ^{31}P-1D spectrum of the perdeuterated cUUCGg 14mer RNA recorded at a proton B_0 field strength of 300 MHz and a temperature of 37°C. Parameters were set as follows: 1,024 scans, 3 s recycling delay and 1.7 s acquisition time. **c** R_1 relaxation rates of the cUUCGg 14mer RNA measured at a proton B_0 field strength of 600 MHz and a temperature of 37°C. R_1 relaxation rates for the protonated sample are depicted as *filled squares* connected by a *solid line*. R_1 relaxation rates for the perdeuterated sample are depicted as *filled triangles* connected by a *dashed line*

blue. 1× running buffer contained 50 mM Tris-acetate and 50 mM sodium phosphate (pH 8.3). The gel was cast using 15% acrylamide with an acrylamide:bisacrylamide ratio of 37.5:1. Running conditions were set as follows: $U = 70$ V, $P < 0.5$ W for 4 h, water cooling to prevent heating. The gel was stained with ethidium bromide.

Liquid-state NMR spectroscopy

NMR measurements were performed on three different Bruker NMR spectrometers, a 300 MHz spectrometer equipped with a 5 mm BBO z-gradient probe, a 600 MHz spectrometer equipped with a 5 mm cryogenic HCP z-gradient probe, and a 900 MHz spectrometer equipped with a 5 mm HCP xyz-gradient probe. Transversal and longitudinal relaxation data were obtained using modified Bruker standard pulse sequences for R_1 (t1ir) and R_2 (cpmg) relaxation rate determination. The carrier frequency was set to 0.61 ppm on the phosphate buffer signal. To suppress the buffer signal, moderate presaturation with $\gamma B_1/2\pi = 2.5$ Hz was applied during the magnetization recovery delay of the cpmg and the t1ir pulse sequences and during the variable R_1 relaxation delay of the t1ir pulse sequence. R_1 relaxation data were acquired with a recycling delay of 10 s. At 900 MHz (364.4 MHz; ^{31}P), 16 increments with 480 scans each, at 600 MHz (242.8 MHz; ^{31}P), 16 increments with 224 scans each and at 300 MHz (121.4 MHz; ^{31}P), 18 increments with 512 scans each were used to determine R_1. R_2 relaxation data were acquired with 12 relaxation delay increments with 640 scans (600 MHz) and 1,696 scans (300 MHz) each. A constant CPMG field of 50 Hz was applied during the R_2 relaxation period. The recycling delay was set to 3 s. The resonance assignments of the ^{31}P nuclei at 25°C were taken from Fürtig et al. (Fürtig et al. 2004). The resonance assignments at 37°C were obtained by recording an HCP experiment with a uniformly ^{13}C, ^{15}N-labeled cUUCGg tetraloop 14mer RNA sample and transferring this assignment to the assignment at 25°C.

Solid-state NMR spectroscopy

Measurements were performed on a Bruker 400 MHz spectrometer equipped with a Bruker 4 mm DVT HXY probe head. ^{31}P-CP MAS spectra were acquired using a ^{1}H 90° excitation pulse of 2.5 μs. The CP contact time was optimized to 1,500 μs (RNA as freeze-dried powder) and 2,500 μs (RNA in frozen buffer), respectively. ^{1}H decoupling (Spinal64) (Fung et al. 2000) was applied during acquisition with a field strength of 70 kHz. The recycling delay was set to 2 s. All spectra were recorded with an MAS spinning rate of 2,000 or 3,000 Hz, respectively.

Data analysis

Solid-state NMR spectra

The size of the ^{31}P CSA tensor was determined by analyzing the MAS spinning sideband intensities using the lineshape analysis algorithms integrated in Topspin 2.1 (Bruker, Germany). The line width of the ^{31}P spectra was determined within the ^{31}P tensor fitting procedure. It represents the average line width of the isotropic peak and all sidebands.

From the ^{31}P tensor, the magnitude of the CSA was calculated using (Hansen and Al-Hashimi 2006)

$$\mathrm{CSA} = \sqrt{1.5\left[(\delta_{11} - \delta_{\mathrm{iso}})^2 + (\delta_{22} - \delta_{\mathrm{iso}})^2 + (\delta_{33} - \delta_{\mathrm{iso}})^2\right]} \quad (1)$$

Liquid-state NMR spectra

Spectra were processed and analyzed using Topspin 2.1 (Bruker, Germany). R_1 and R_2 relaxation rates were fit from peak heights to two-parameter monoexponential functions with the Software Sigma Plot 10.0 (Systat Software GmbH, Germany).

The obtained relaxation parameters were further analyzed using the program modelfree 4.20 (Mandel et al. 1995). This program uses the modelfree formalism introduced by Lipari and Szabo (1982a, b) and modified by Clore et al. (1990). The dipolar relaxation term was set to zero during the analysis. Model selection was achieved according to d′Auvergne and Gooley (2003) using Akaike's information criterion (AIC). The AIC is given by

$$\mathrm{AIC} = \chi^2 + 2k \quad (2)$$

k is the number of modelfree parameters in the model.

The overall rotational correlation time τ_c was optimized during the modelfree fitting procedure and finally compared to the outcome of a hydrodynamic calculation using the program hydronmr 5a (Garcia de la Torre et al. 2000). Rotational diffusion was assumed to be either isotropic or axially symmetric. In case of axially symmetric diffusion, the CSA tensor was oriented along the P-O3′ bond. This assumption differs by only 7° from the orientation of the CSA tensor of barium diethylphosphate (Herzfeld et al. 1978). The initial diffusion tensor used for the modelfree fitting was calculated on the basis of our NMR structure of the cUUCGg tetraloop 14mer RNA (Nozinovic et al. unpublished results) using the program hydronmr 5a (Garcia de la Torre et al. 2000). During the modelfree calculations, the diffusion tensor was allowed to adjust in size and orientation. R_1 relaxation rates recorded at magnetic fields of 300 MHz (121.4 MHz; ^{31}P), 600 MHz (242.8 MHz; ^{31}P) and 900 MHz (364.4 MHz; ^{31}P) and the

R_2 relaxation rates recorded at 600 MHz (242.8 MHz; ^{31}P) were used as input data for the modelfree calculation.

Results and discussion

R_1 and R_2 relaxation in solution are caused by fluctuations in the local magnetic field surrounding the NMR-active nuclei. For RNA, these fluctuations are mainly caused by CSA and dipolar contributions. Dipolar contributions to the relaxation of ^{15}N- or ^{13}C-nuclei are dominated by covalently bound proton nuclei. In the case of ^{31}P in the phosphodiester backbone of oligonucleotides, no directly bound proton is present but the ^{31}P nucleus experiences the influence of various hydrogens that are three or four bonds apart (H3′, H4′ H5′, H5″, H2′). Therefore, separation of these two contributions is a prerequisite for the analysis of the autocorrelated relaxation rates of the ^{31}P nuclei of the phosphodiester backbone of RNA. Magusin et al. (Magusin and Hemminga 1994) calculated the contribution of dipolar relaxation in R_2 to be 37% at a proton magnetic field strength of 300 MHz and 18% at a proton magnetic field strength of 500 MHz. Consequently, the dipolar relaxation mechanisms in protonated RNA molecules cannot be neglected.

Dipolar relaxation terms

The dipolar interaction shows an r^{-6}-dependence on the distance between the two interacting nuclei. Therefore, it is crucial to know the exact distance between the nuclei. The fact that the protons causing dipolar relaxation are at least 3 bonds with flexible torsions (α, β; ε, ζ; α, β, γ; pseudorotation phase P) apart from ^{31}P nuclei in the phosphodiester backbone of an RNA makes it difficult to determine exact ^{1}H-^{31}P distances. Therefore, the magnitude of the dipolar relaxation contributions in protonated RNA samples to the ^{31}P R_1 and R_2 relaxation rates are difficult to define.

In order to determine the dipolar contributions to R_1 relaxation rates, we compared data from R_1 relaxation measurements for a protonated and a perdeuterated cUUCGg tetraloop 14mer RNA (Fig. 1a). In this tetraloop, the ^{31}P signals are resolved in the ^{31}P-1D spectrum (see 1D spectrum recorded at a proton B_0 field strength of 300 MHz in Fig. 1b), making it possible to determine the ^{31}P relaxation rates directly on the ^{31}P spins without magnetisation transfer from other nuclei using e.g. HCP (Marino et al. 1994) (Heus et al. 1994), HCP-CCH-TOCSY (Marino et al. 1995) or HP-TOCSY (Kellogg 1992) experiments. The comparison of the R_1 relaxation rates determined at a temperature of 37°C is shown in Fig. 1c. R_1 relaxation rates of the protonated RNA are 0.4 Hz higher on average than for the perdeuterated RNA. Hence, this difference is caused by the sum of all ^{1}H–^{31}P dipolar relaxation contributions because ^{2}H–^{31}P dipolar relaxation in the perdeuterated sample should be scaled down by a factor of 16, taking into account the lower gyromagnetic constants and the difference in spin quantum number of ^{2}H ($\gamma_D = 4.11*10^7 T^{-1}s^{-1}$; $I_D = 1$) compared with ^{1}H ($\gamma_H = 26.75*10^7 T^{-1}s^{-1}$, $I_H = 1/2$). We calculate a maximum ^{2}H–^{31}P relaxation rate of 0.02 Hz, an effect we are not able to detect given the experimental error of our measurements.

CSA relaxation terms

In a perdeuterated RNA, the ^{31}P nuclei of the phosphodiester backbone can be treated as isolated spins and, when care has been taken to exclude paramagnetic impurities, only the CSA of the ^{31}P nucleus causes its R_1 relaxation. R_2 relaxation rates are caused by CSA relaxation and chemical exchange contributions. Hence, by analyzing both R_1 and R_2, CSA relaxation terms can be separated from chemical exchange terms.

If the rotational diffusion of the RNA is isotropic, then the CSA contribution to R_1 and R_2 relaxation is only dependent on the size but not on the orientation of the CSA. However, if one assumes an axially symmetric diffusion tensor, the relaxation depends on the orientation of the CSA tensor with respect to the diffusion tensor of the RNA molecule. This orientation can only be determined, if the orientation of the CSA tensor within the molecular frame of the phosphodiester backbone as well as the conformation of the phosphodiester backbone with respect to the overall shape of the molecule is known.

The ^{31}P CSA tensor: size and orientation

The orientation of the ^{31}P CSA tensor within the molecular frame was determined for barium diethyl phosphate as a model compound mimicking the phosphodiester backbone (Herzfeld et al. 1978). However, the size of the principal axis values of the CSA tensor can be dependent on the conformation of the phosphodiester backbone. For example, such CSA tensor dependence has been reported for ^{15}N nuclei in the backbone of proteins (Fushman et al. 1998; Kroenke et al. 1999; Loth et al. 2005; Hall and Fushman 2006).

In the seventies, the size of the principal axis values of the ^{31}P CSA tensor for RNA molecules were determined by solid-state NMR measurements for polyU, polyG, polyC, polyA and tRNA (Terao et al. 1977). From these values, the CSA magnitude according to Eq. 1 calculates to 172.0 ppm (tRNA), 174.7 ppm (polyU), 182.0 ppm (polyC), 173.2 ppm (polyG), 175.8 ppm (polyA). For double stranded DNA, a phosphate CSA magnitude of 157.8 ppm could be

derived from solid state NMR measurements (Heisaburo 1980). This CSA value is significantly smaller than the CSA values reported for RNA. Since tRNA adopts predominantly A-form helical conformation for most of the nucleotides, an averaged value of 172 ppm was proposed to represent the valid CSA value for RNA molecules. However, there seems to be quite some difference in the size of the CSA between these different molecules. Since polyN RNAs are supposed to assume ensembles of random structures, these differences are most intuitively explained by a pronounced dependence of the CSA on the average conformation of the phosphodiester backbone that then has to be different for different homopolymeric oligonucleotides. Recently performed DFT studies of the conformational dependence of the ^{31}P CSA tensor in the phosphodiester backbone of DNA and RNA molecules further support this interpretation. Taking the principal axis values from the DFT study, the CSA magnitude calculates to 176.5 ppm for RNA (Precechtelova et al. 2008). On the other hand, the dispersion of isotropic chemical shift of ^{31}P in the phosphodiester backbone is very small ($\sigma_{CS} = \pm$ 1.5–2 ppm) (BMRB database), which indicates a small conformational dependence of the ^{31}P CSA.

We conducted ^{31}P solid-state NMR measurements on a GC 20mer duplex RNA in order to determine the ^{31}P CSA magnitude for the relaxation analysis in solution. We controlled by polyacrylamide gels that the duplex was exclusively formed. Therefore, all nucleotides in this duplex are supposed to adopt similar A-form helical conformations and induce a very similar electronic environment for each ^{31}P nucleus. ^{31}P-1D CP MAS spectra were recorded under a variety of different conditions changing salt concentration, humidity and temperature. The spectra were fit and principal axis values of the ^{31}P CSA tensor were determined. Figure 2 shows exemplarily a ^{31}P-1D CP MAS solid-state NMR spectrum of the freeze-dried GC-20mer duplex RNA in the absence potassium chloride (KCl) measured at a proton carrier frequency of 400 MHz (161.976 MHz, ^{31}P) and a temperature of 250 K. In green, the simulated spectrum assuming one single ^{31}P CSA tensor is shown. Apparently, the assumption of a single ^{31}P CSA tensor is sufficient to precisely simulate the experimental spectrum. Accordingly, the 38 ^{31}P nuclei in the complex either assume very similar conformations or the conformational dependence of the CSA tensor is small. We analyzed the ^{31}P CSA for different KCl concentrations and temperatures and investigated the differences between freeze-dried RNA and RNA measured in frozen buffer. The results are summarized in Table 1.

In ice, the ^{31}P CSA is 160.5 ppm and is not dependent on varying KCl concentrations. In contrast, the ^{31}P CSA is much larger for freeze-dried RNA samples and shows a dependence on the KCl concentration, albeit not in the physiological concentration range. The CSA value

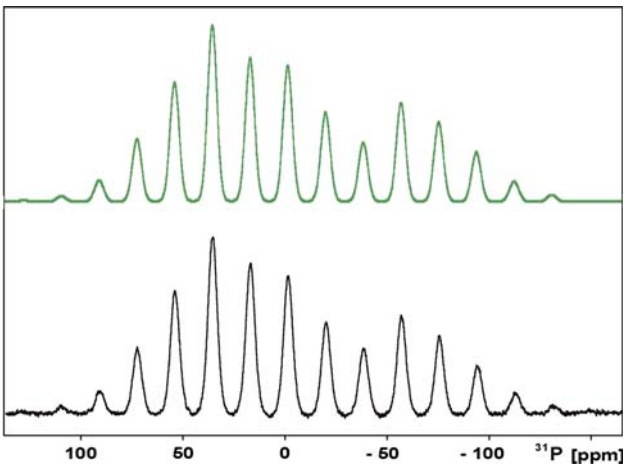

Fig. 2 ^{31}P-1D CP MAS solid-state NMR spectrum of the freeze-dried GC-20mer duplex RNA without KCl measured at a proton B_0 field of 400 MHz and a temperature of 250 K (*black line*). Acquisition parameters were set as follows: MAS rotation frequency 3 kHz, CP contact time 1.5 ms, ^{1}H decoupling field strength 70 kHz, recycling delay 2 s, scans 6,400. The chemical shift of the isotropic signal is −1.5 ppm. The *green line* represents the simulated spectrum. The principal axis values of the ^{31}P CSA tensor derived from the simulation are given in Table 2

increases with the salt concentration from 178.5 ppm in the absence of KCl to 188.9 ppm for 1 M KCl. If the freeze-dried sample is equilibrated to 84% air humidity, the CSA reduces to 157.4 ppm.

It was reported previously for collagen fibrils (Reichert et al. 2004) that fast to intermediate time scale dynamics affect the apparent CSA value determined by solid-state NMR measurements. These dynamics can be expressed by an order parameter S which scales the unperturbed CSA value. For collagen fibrils, S depends on the hydration level. Odahara et al. (1994) reported the dependence of the ^{31}P CSA tensor on temperature in pelleted ribosome samples as well as the dependence of the ^{31}P CSA tensor of calf thymus DNA on relative air humidity and temperature. The homogenous line width of the side bands of tobacco mosaic virus (TMV) samples was determined to be 90 Hz, while the inhomogeneous line width greatly differs with a pronounced dependence on the water content of the sample (Hemminga et al. 1987). This inhomogeneous line broadening was interpreted as conformational heterogeneity that is averaged out in samples with higher water content. Finally, Magusin and Hemminga (1993, 1994) performed a detailed relaxation and CSA tensor analysis on M13 virus as well as on TMV samples. In this study, the change in line width was interpreted as arising from fast restricted fluctuations of the dihedral angles in the phosphodiester backbone. Taken together, due to dynamics on the μs time scale, the size of the principal axis values of the observed ^{31}P CSA tensor as well as the line width of the sidebands depend strongly on sample preparation.

Table 1 Experimental ^{31}P chemical shift tensor principal values, the corresponding isotropic chemical shift values, the CSA values calculated according to Eq. 1 and the line widths extracted from the CSA fits

Sample	KCl (mM)	T (K)	δ_{11} (ppm)	δ_{22} (ppm)	δ_{33} (ppm)	δ_{iso} (ppm)	CSA (ppm)	Line width (Hz)
Ice[a]	0	250	79.8	17.8	−102.7	−1.68	160.7	313
Ice[a]	50	250	79.2	17.6	−101.9	−1.68	159.5	315
Ice[a]	100	250	80.4	17.6	−103.1	−1.73	161.5	298
Ice[a]	1,000	250	79.4	18.1	−102.4	−1.60	160.2	308
Freeze-dried[b]	0	250	86.4	23.8	−115.0	−1.61	178.4	979
Freeze-dried[b]	500	250	88.6	25.6	−119.4	−1.73	184.8	989
Freeze-dried[b]	1,000	250	89.9	27.5	−122.3	−1.63	188.9	987
Freeze-dried[b]	100	310	85.8	22.2	−111.5	−1.18	174.4	723
84% humid[c]	100	310	79.1	17.0	−99.8	−1.24	157.4	403

Data were obtained on GC-20mer duplex RNA samples under different salt concentrations and at different temperatures

[a] RNA sample measured in frozen buffer

[b] Freeze-dried sample (corresponds to 0% air humidity)

[c] Freeze-dried sample equilibrated to 84% air humidity

In the case of the GC 20mer duplex RNA, 84% air humidity seems to introduce dynamics of the phosphodiester backbone, thereby reducing the order parameter and the apparent CSA from 174.4 ppm to 157.4 ppm. In line with this observation, the line width diminishes from 723 to 403 Hz. If one compares these values to the CSA tensor values obtained for RNA samples measured in ice, the reduction in both CSA and line width indicates that the phosphodiester backbone of RNA samples in ice experiences significant dynamics. The effects on CSA and line width are consistent: the smaller the magnitude of the CSA, the smaller the line width. Consequently, we can conclude that the CSA value representing a static case has to be larger or equal to 178.5 ppm.

There are two possible explanations for the observed dependence of the CSA on the KCl concentrations of freeze-dried RNA samples. It might be possible that K^+ cations influence the electron density around the ^{31}P nucleus. This effect would only be present if cations come very close to the ^{31}P nucleus, like in the freeze-dried state of the RNA. In this case, 178.5 ppm is the correct CSA magnitude because in solution at 50 mM KCl the mean distance between K^+ ion and phosphate group is too large to cause such an effect. Alternatively, the KCl dependence could arise from a dynamic effect where small K^+ and Cl^- ions fill up gaps between phosphodiester backbone sides in the RNA and thereby stiffen the phosphodiester backbone. In this case, a CSA value of 188.9 ppm determined at high KCl concentrations in the freeze-dried state would be valid for the relaxation analysis in solution.

We consider the K^+ ions influence on the electron density of the phosphate group to be the more likely explanation, since there is no further increase in line width upon an increase of KCl in the freeze-dried state. Therefore, we performed the analysis of the liquid-state NMR data with a CSA magnitude of 178.5 ppm. However, we also examined the effect of different ^{31}P CSAs on the outcome of the modelfree analysis.

Our data show that the CSA magnitudes determined on freeze-dried RNA samples depend strongly on sample preparation. This dependence on sample preparation might explain the large differences in CSA magnitudes for the phosphodiester backbone determined by solid-state NMR previously. In our opinion, the conformational dependence of the CSA is small judged by the small chemical shift dispersion observed in solution, at least for the allowed backbone angle combinations. Therefore, we assumed a constant CSA value of 178.5 ppm for all phosphodiester ^{31}P nuclei within the cUUCGg 14mer RNA, which is very close to the CSA value determined by DFT calculations for A-form RNA (Precechtelova et al. 2008). In proteins, the isotropic chemical shift dispersion for the backbone ^{15}N nuclei is 25–30 ppm. However, the conformational dependence of the ^{15}N CSA was found to be only 5–10% (Kroenke et al. 1999; Loth et al. 2005). Therefore, relaxation analysis in proteins is usually performed with the assumption of a constant ^{15}N CSA value. In RNA the chemical shift dispersion of the phosphodiesters is only ±1.5-2 ppm. (BMRB database). Although the conformational dependence of the ^{31}P CSA has not yet been determined experimentally, it is presumably much smaller than the conformational dependence of the backbone ^{15}N CSA in proteins. Hence, the assumption of a constant CSA value for all phosphodiester nuclei is likely to lead to reasonable results.

Relaxation analysis of the perdeuterated RNA

Figure 3a, b show representative ^{31}P relaxation decay curves for R_1 and R_2 at a proton B_0 field strength of 600 MHz and 37°C. These curves can be fitted

monoexponentially, indicating that the RNA sample preparation is homogenous and monomeric. R_1 relaxation rates were determined for a perdeuterated cUUCGg tetraloop 14mer RNA solubilized in a 100% D_20 buffer at different proton B_0 magnetic field strengths of 300, 600 and 900 MHz (Fig. 3c) at a temperature of 37°C. As expected for molecules with an overall tumbling rate τ_c around 2 ns, R_1 relaxation rates increase with B_0 magnetic field strength. However, this field dependence seems to be different for some of the ^{31}P nuclei. For instance, the R_1 relaxation rates of the phosphates p2, p10 and p14 show a higher B_0 field dependence than the other ^{31}P nuclei. Apparently, the loop phosphates p7 and p9 show small R_1 relaxation rates while p8 shows a high R_1 relaxation rate when compared at the same B_0 field strength. This characteristic trend is prominent at 300, 600 and 900 MHz (Table S3, Supplementary Material).

R_2 relaxation rates were determined at proton B_0 magnetic field strengths of 300 MHz (Table S3, Fig. S2, Supplementary Material) and 600 MHz at a temperature of 37°C (Fig. 3d; Table S3, Supplementary Material). The R_2 relaxation rates recorded at 600 MHz lie between 9.6 and 11.8 Hz, while the phosphates of the hairpin loop p7, p8, p9, p10 show slightly lower R_2 rates than the other phosphates. The only exception is p2 which has a significantly higher R_2 relaxation rate (14.75 Hz). Furthermore, this p2 signal appears to be weaker and broader than all other phosphate signals in the ^{31}P-1D (Fig. 1b) spectrum. This observation suggests a significant chemical exchange contribution to the R_2 relaxation rate of phosphate p2.

Modelfree analysis

As input data for the modelfree analysis, R_1 relaxation rates recorded at proton B_0 magnetic field strengths of 300, 600 and 900 MHz and R_2 relaxation rates recorded at a proton B_0 magnetic field strength of 600 MHz at 37°C were used. The R_2 relaxation rates recorded at a proton B_0 magnetic field strength of 300 MHz were not used as input, but as cross validation data of the selected motional model (Fig. S2, Supplementary Material). The results of the model-free analysis assuming a ^{31}P CSA magnitude of 178.5 ppm are summarized in Table 2. Modelfree parameters S^2, S_s^2, S_f^2, τ_e, R_{ex} and the selected model are given for an isotropic as well as for an axially symmetric rotational diffusion tensor.

In addition, the modelfree analysis was performed assuming ^{31}P CSA magnitudes of 168 and 188.9 ppm, respectively. The modelfree parameters are given in Table S1 (CSA = 168 ppm), and Table S2 (CSA = 188.9 ppm) of the Supplementay Material. Figure 4 shows the S^2 order parameters extracted from the modelfree analysis for different CSA values of 168, 178.5 and 188.9 ppm assuming isotropic rotational diffusion. In addition, the S^2 values for

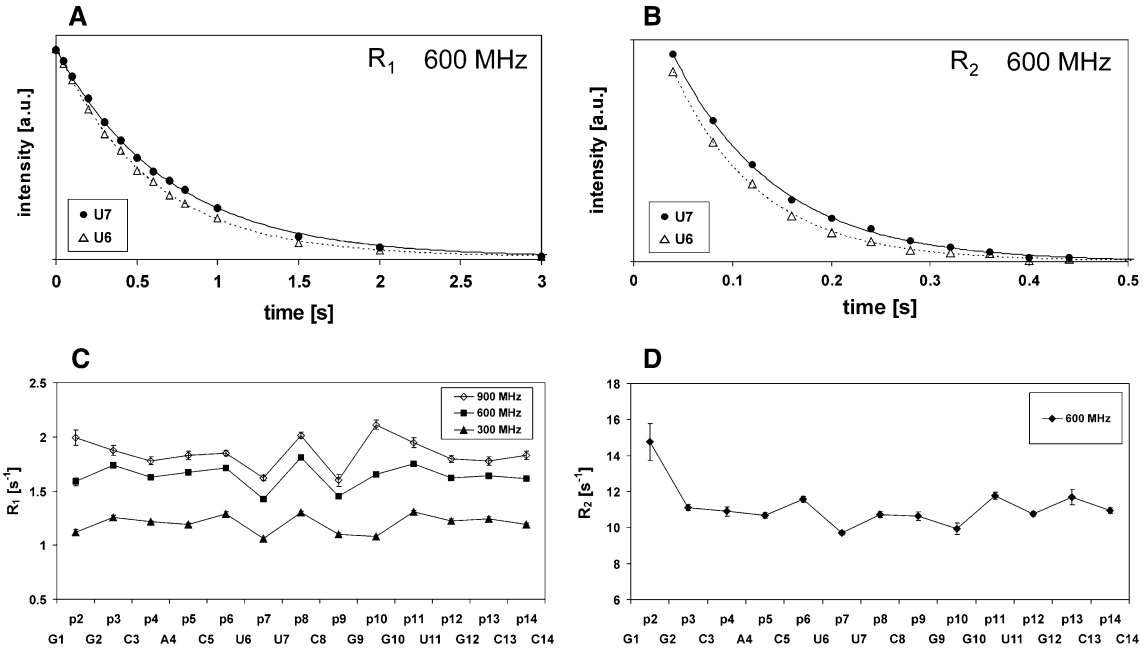

Fig. 3 **a** R_1 relaxation decay *curves* for the ^{31}P nuclei p6 and p7 at a proton B_0 field strength of 600 MHz and a temperature of 37°C. Peak intensities are plotted against the relaxation delay. **b** R_2 relaxation decay *curves* for the ^{31}P nuclei p6 and p7 at a proton B_0 field strength of 600 MHz and a temperature of 37°C. Peak intensities are plotted against the relaxation delay **c** R_1 relaxation rates of the ^{31}P nuclei of the cUUCGg 14mer RNA measured at different proton B_0 field strengths of 300 MHz (*filled triangles*), 600 MHz (*filled squares*) and 900 MHz (*open circles*) at a temperature of 37°C. **d** R_2 relaxation rates of the ^{31}P nuclei of the cUUCGg 14mer RNA measured at a B_0 field strength of 600 MHz at a temperature of 37°C

Table 2 Results of the ^{31}P modelfree analysis of the cUUCGg tetraloop RNA

	S^2	S_s^2	S_f^2	τ_e (ps)	$R_{ex}(s^{-1})$	Rotational diffusion	Model
p2-G2	0.695 ± 0.022			79.9 ± 11.3	4.95 ± 1.46	Iso	4
	0.690 ± 0.022			73.2 ± 11.3	5.25 ± 1.46	Aniso	4
p3-C3	0.778 ± 0.036	0.928 ± 0.041	0.839 ± 0.011	1,300 ± 1,167		Iso	5
	0.821 ± 0.022			34.4 ± 12.2		Aniso	2
p4-A4	0.795 ± 0.009			26.2 ± 8.7		Iso	2
	0.796 ± 0.009			25.4 ± 8.7		Aniso	2
p5-C5	0.748 ± 0.020	0.928 ± 0.020	0.807 ± 0.012	786 ± 553		Iso	5
	0.745 ± 0.02	0.924 ± 0.022	0.806 ± 0.012	840 ± 563		Aniso	5
p6-U6	0.847 ± 0.011			23.1 ± 11.1		Iso	2
	0.847 ± 0.011			23.6 ± 11.0		Aniso	2
p7-U7	0.691 ± 0.009			24.2 ± 4.8		Iso	2
	0.682 ± 0.011			22.5 ± 5.1	0.42 ± 0.24	Aniso	4
p8-C8	0.662 ± 0.088	0.780 ± 0.103	0.849 ± 0.009	2,915 ± 1,522		Iso	5
	0.670 ± 0.087	0.790 ± 0.102	0.849 ± 0.009	2,872 ± 1,552		Aniso	5
p9-G9	0.733 ± 0.007				0.58 ± 0.38	Iso	3
	0.741 ± 0.006					Aniso	1
p10-G10	0.663 ± 0.014			110.9 ± 9.2		Iso	2
	0.654 ± 0.015			106.4 ± 9.5	0.49 ± 0.27	Aniso	4
p11-U11	0.855 ± 0.009			45.9 ± 14.6		Iso	2
	0.850 ± 0.010			30.0 ± 15.3	0.33 ± 0.24	Aniso	4
p12-G12	0.790 ± 0.009			29.8 ± 7.7		Iso	2
	0.792 ± 0.009			22.7 ± 8.0		Aniso	2
p13-C13	0.830 ± 0.006					Iso	1
	0.826 ± 0.006					Aniso	1
p14-C14	0.779 ± 0.008			37.2 ± 7.7		Iso	2
	0.779 ± 0.008			41.1 ± 7.7		Aniso	2
	$\tau_c = 1.926$					Iso	
	$\tau_c = 1.908$	$D_{aniso} = 1.153$				Aniso	

The CSA value was set to 178.5 ppm. The analysis was performed with the assumption of either an isotropic or an axially symmetric rotational diffusion tensor, respectively

a CSA value of 178.5 ppm assuming axially symmetric rotational diffusion are illustrated.

A comparison of the S^2 parameters for the different CSA values (Fig. 4) shows that for fitting the relaxation data to the Lipari Szabo model the S^2 parameters and the CSA values are inversely correlated. However, a comparison of the individual ^{31}P nuclei reveals that the relative trend for the S^2 values remains unchanged. The CSA simply scales the S^2 order parameters even without changing model selection, τ_c, R_{ex} or S_s^2. However, ^{31}P nuclei described by model 2 experience minor shifts of τ_e towards longer timescales in case of smaller CSA values. It is not possible to discriminate between different CSA magnitudes by statistical methods since the final residual errors are comparable in size ($\chi^2 = 11.89$ (CSA = 188.9 ppm), $\chi^2 = 11.98$ (CSA = 178.5 ppm) and $\chi^2 = 12.42$ (CSA = 168 ppm)). However, as discussed above, our solid-state NMR data indicate that assuming a CSA value of 178.5 ppm is reasonable.

A global rotational correlation time τ_c of 1.926 ns derived from the modelfree analysis is in good agreement with hydrodynamic calculations performed with the program hydronmr 5a ($\tau_c = 1.94$ ns) using the NMR solution structure of the cUUCGg tetraloop 14mer RNA (Nozinovic et al. unpublished results).

We analyzed the effect of anisotropic rotational diffusion on the results of the modelfree analysis. Comparison of the isotropic versus the axially symmetric diffusion model (Table 2; Fig. 4) clearly shows that there are only small differences in the final result of the modelfree analysis for the 14mer RNA with an asymmetry of the rotational diffusion tensor of $\sim$1.2. Residual overall errors are comparable with $\chi^2 = 11.98$ (CSA = 178.5 ppm) for the isotropic and $\chi^2 = 12.54$ (CSA = 178.5 ppm) for the

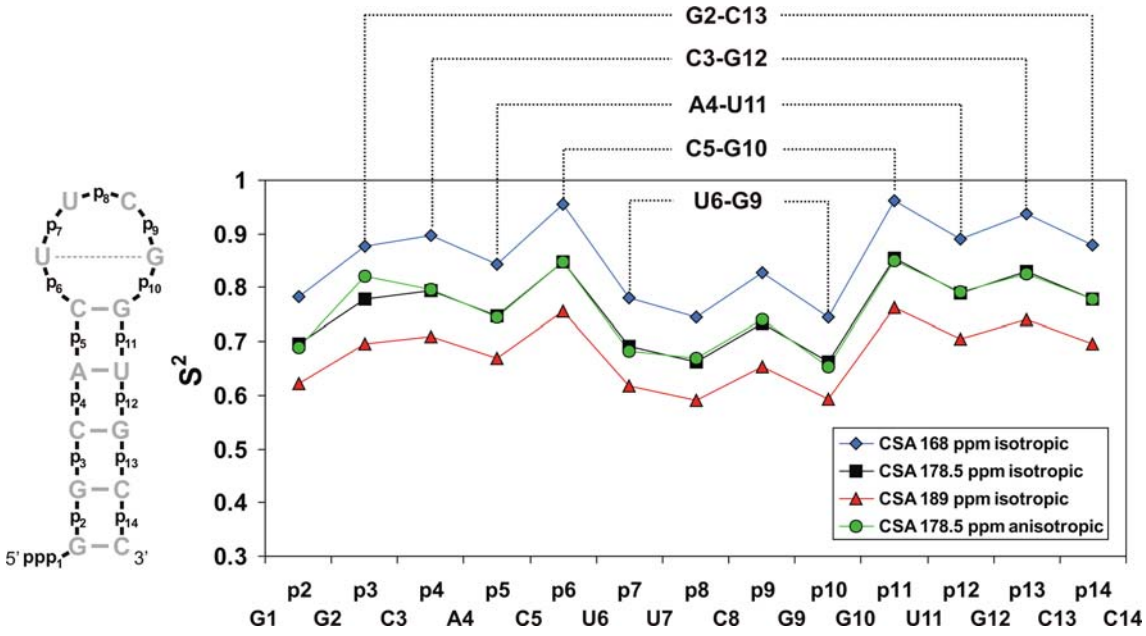

Fig. 4 S^2 order parameters for the ^{31}P nuclei in the cUUCGg tetraloop 14mer RNA determined at a temperature of 37°C. S^2 parameters are depicted for different CSA values of 168 ppm (*blue*), 178.5 ppm (*black*) and 189 ppm (*red*). For a CSA value of 178.5 ppm, the effect of isotropic (*black*) versus anisotropic (*green*) rotational diffusion is illustrated. S^2 parameters of ^{31}P nuclei located on the 3′ side with respect to base pairs are connected by *dotted lines*

anisotropic model. Only p3 exhibits a larger deviation which can be explained by a different model selection for the anisotropic fit.

S^2 values obtained by the modelfree analysis with a CSA of 178.5 ppm lie between 0.66 and 0.86. ^{31}P nuclei p2, p7, p8, p9, p10 exhibit lower S^2-values than the average. The phosphate p2 is located next to the closing base pair of the hairpin stem while p7, p8, p9, p10 are located in the hairpin loop of the 14mer RNA presumably explaining why phosphodiester backbone flexibility seems to be more pronounced in these regions of the 14mer RNA molecule. Highest S^2 values are obtained for p6 ($S^2 = 0.847$) and p11 ($S^2 = 0.855$). While p11 is located within the A-helix of the RNA hairpin next to the stable GC base pair, p6 is located within the cUUCGg tetraloop. The dynamics of the phosphodiester backbone appear to be significantly influenced by the dynamics of the 5′ neighboring nucleotide and not by the 3′ neighboring nucleotide. This observation would also explain why p2 ($S^2 = 0.695$) has a significantly lower S^2 than p14 ($S^2 = 0.779$). Furthermore, the flexibility of a certain base pair seems to influence the flexibility of the 3′ adjacent phosphodiester groups (Fig. 4).

Most of the phosphodiesters exhibit a fast motional component on a timescale between $\tau_e = 22$ ps and $\tau_e = 111$ ps. Only phosphates p9 and p13 show flexibility that is faster than 20 ps. The sum of angular fluctuations of the phosphodiester angles α, β, γ, ε and ζ within one conformation are thought to be the reason for this fast time scale motion. In addition, p3 and p5 show motion on a slower time scale. This motion has small amplitude and a τ_e around 1 ns. In contrast, p8 exhibits high amplitude motion on an even slower timescale. Conformational transitions between the two most stable sugar pucker conformations C2′-endo and C3′-endo is on a time scale around 1 ns while changes in phosphodiester backbone conformation for the angles α, β, γ, ε and ζ are either not observed at all or on a time scale of tens of nanoseconds as reported for MD simulations performed on ApA, ApC, CpA and CpC dinucleoside monophosphates (Vokacova et al. 2009). From this MD study, Vokacova et al. could show that transitions between different phosphodiester backbone conformations occur as concerted flips of the backbone angles. This strong mutual correlation might explain why these transitions are comparably slow. Nevertheless, angular fluctuations within one backbone conformation were observed for all backbone angles with amplitudes of 30°–40°. These fluctuations may explain the fast time scale motion obtained from the modelfree analysis of the phosphate groups in our study of the cUUCGg tetraloop 14mer RNA. The small amplitude motion reported for the nucleotides C3 and C5 might be due to conformational dynamics in the sugar pucker conformation of one of the adjacent sugars. A change in sugar conformation would only cause a small angular rearrangement of the phosphate group and such a conformational change is known to occur on the same timescale. Phosphate p8 experiences motions on a slower time scale and of larger amplitude than p3 and p5. p8 is the most exposed

phosphate within the cUUCGg tetraloop 14mer RNA and is supposed to be the most flexible one. It might be that this phosphodiester group is an exception to the rule and conformational backbone rearrangement for p8 is on a timescale of low ns regime.

Phosphate p2 experiences a significant chemical exchange contribution of $R_{ex} = 5.0 \pm 1.5$. This phosphate is located 3′ of G1 which participates in the closing base pair of the 14mer hairpin RNA. Indeed, it has been reported earlier that ^{31}P nuclei experiencing chemical exchange on the millisecond timescale can be correlated to base pair lifetimes in duplex DNA (Catoire 2004). Imino-1D spectra recorded on an H_20 sample of the cUUCGg tetraloop 14mer RNA at different temperatures show significant line broadening, suggesting destabilization of the G1–C14 base pair at $T = 37$°C (Nozinovic et al. unpublished results).

Conclusion

We have measured ^{31}P relaxation rates and analyzed these rates following the Lipari-Szabo formalism for a 14mer cUUCGg tetraloop RNA. The cUUCGg tetraloop represents the most stable tetraloop motif and its dynamic properties have previously been investigated (Duchardt and Schwalbe 2005; Shajani and Varani 2005; Vallurupalli and Kay 2005; Ferner et al. 2008) for the base and the sugar moieties. This model hairpin therefore represents an ideal model system to measure ^{31}P relaxation properties for each phosphate along the phosphodiester backbone for the first time. Such site resolution could be achieved due to favorable dispersion in the ^{31}P chemical shifts of the cUUCGg tetraloop. For larger RNA molecules, measurement of ^{31}P relaxation properties with site resolution, however, becomes feasible, when selective deuteration schemes such as H1′,D2′,D3′,D4′,D5′,D5″-labeled nucleotides are used and if P–C–H coherence transfer schemes are applied to resolve individual ^{31}P resonances in the H1′–C1′ two dimensional plane of such experiments.

As previously predicted (Magusin and Hemminga 1994), ^{31}P relaxation is influenced by H–P dipolar contributions in protonated RNAs. In order to eliminate this distance-dependent effect, we performed our R_1 and R_2 relaxation analysis using a perdeuterated sample of the tetraloop RNA. For the interpretation of the relaxation rates in the context of the modelfree formalism, it is essential to know size and, in case of anisotropic rotational diffusion, also the orientation of the ^{31}P CSA tensor. In order to address the first part, we performed solid-state NMR experiments and showed that there is a pronounced dependence of the CSA on hydration. This effect can be explained by dynamics on the ns to μs timescale and is in agreement with previous ^{31}P solid-state NMR studies performed on TMV (tobacco mosaic virus) and M13 virus samples (Hemminga et al. 1987; Magusin and Hemminga 1993, 1994). Furthermore, we discovered changes in the CSA upon addition of 1 M KCl for RNA samples in the freeze-dried state. Based on our analysis, we propose a value of 178.5 ppm for the ^{31}P CSA in the static case.

On the basis of this CSA, we observed that, with exception of the flexible nucleobase U7, the phosphodiester backbone is more flexible than the ribose (C1′–H1′) and the nucleobase (C8–H8, C6–H6) moieties (Duchardt and Schwalbe 2005; Ferner et al. 2008). Furthermore, the dynamics of the phosphodiester backbone appear to be significantly influenced by the dynamics of the 5′ neighboring nucleotide (Fig. 4). Order parameters derived from MD simulations have proven to be consistent with NMR derived order parameters of the CH bond vectors in the ribose and the nucleobase moieties. It will be the subject of future investigations to see whether MD simulations are also able to reproduce the results obtained by means of NMR spectroscopy concerning the dynamics of the phosphodiester backbone. Such investigation will be helpful to understand the dynamic properties of RNA molecules, especially for the dynamic hinge defined by rotation around the ζ, α torsions of RNA.

Acknowledgments The work has been supported by the state of Hesse (Center for Biomolecular Magnetic Resonance, BMRZ) and the DFG (Sonderforschungsbereich 579: RNA-ligand-interactions). H·S. and C.G. are members of the DFG Cluster of Excellence: Macromolecular Complexes (EXC 115).

References

Akke M, Fiala R, Jiang F, Patel D, Palmer AG 3rd (1997) Base dynamics in a UUCG tetraloop RNA hairpin characterized by ^{15}N spin relaxation: correlations with structure and stability. RNA 3:702–709

Al-Hashimi HM, Walter NG (2008) RNA dynamics: it is about time. Curr Opin Struct Biol 18:321–329

Allain FH, Varani G (1995) Structure of the P1 helix from group I self-splicing introns. J Mol Biol 250:333–353

Blad H, Reiter NJ, Abildgaard F, Markley JL, Butcher SE (2005) Dynamics and metal ion binding in the U6 RNA intramolecular stem-loop as analyzed by NMR. J Mol Biol 353:540–555

Boisbouvier J, Brutscher B, Simorre J, Marion D (1999) 13C spin relaxation measurements in RNA: sensitivity and resolution improvement using spin-state selective correlation experiments. J Biomol NMR 14:241–252

Borer PN, LaPlante SR, Kumar A, Zanatta N, Martin A, Hakkinen A, Levy GC (1994) 13C-NMR relaxation in three DNA oligonucleotide duplexes: model-free analysis of internal and overall motion. Biochemistry 33:2441–2450

Catoire LJ (2004) Phosphorus-31 transverse relaxation rate measurements by NMR spectroscopy: insight into conformational exchange along the nucleic acid backbone. J Biomol NMR 28:179–184

Chowdhury S, Maris C, Allain FH, Narberhaus F (2006) Molecular basis for temperature sensing by an RNA thermometer. EMBO J 25:2487–2497

Clore GM, Szabo A, Bax A, Kay LE, Driscoll PC, Gronenborn AM (1990) Deviations from the simple two-parameter model-free approach to the interpretation of nitrogen-15 nuclear magnetic relaxation of proteins. J Am Chem Soc 112:4989–4991

d'Auvergne EJ, Gooley PR (2003) The use of model selection in the model-free analysis of protein dynamics. J Biomol NMR 25:25–39

Duchardt E, Schwalbe H (2005) Residue specific ribose and nucleobase dynamics of the cUUCGg RNA tetraloop motif by MNMR 13C relaxation. J Biomol NMR 32:295–308

Duchardt E, Nilsson L, Schleucher J (2008) Cytosine ribose flexibility in DNA: a combined NMR 13C spin relaxation and molecular dynamics simulation study. Nucleic Acids Res 36:4211–4219

Ennifar E, Nikulin A, Tishchenko S, Serganov A, Nevskaya N, Garber M, Ehresmann B, Ehresmann C, Nikonov S, Dumas P (2000) The crystal structure of UUCG tetraloop. J Mol Biol 304:35–42

Ferner J, Villa A, Duchardt E, Widjajakusuma E, Wohnert J, Stock G, Schwalbe H (2008) NMR and MD studies of the temperature-dependent dynamics of RNA YNMG-tetraloops. Nucleic Acids Res 36:1928–1940

Ferner J, Suhartono M, Breitung S, Jonker HR, Hennig M, Wohnert J, Gobel M, Schwalbe H (2009) Structures of HIV TAR RNA-ligand complexes reveal higher binding stoichiometries. Chembiochem 10(9):1490–1494

Fung BM, Khitrin AK, Ermolaev K (2000) An improved broadband decoupling sequence for liquid crystals and solids. J Magn Reson 142:97–101

Fürtig B, Buck J, Manoharan V, Bermel W, Jaschke A, Wenter P, Pitsch S, Schwalbe H (2007a) Time-resolved NMR studies of RNA folding. Biopolymers 86:360–383

Fürtig B, Wenter P, Reymond L, Richter C, Pitsch S, Schwalbe H (2007b) Conformational dynamics of bistable RNAs studied by time-resolved NMR spectroscopy. J Am Chem Soc 129:16222–16229

Fürtig B, Richter C, Bermel W, Schwalbe H (2004) New NMR experiments for RNA nucleobase resonance assignment and chemical shift analysis of an RNA UUCG tetraloop. J Biomol NMR 28:69–79

Fushman D, Tjandra N, Cowburn D (1998) Direct measurement of ^{15}N chemical shift anisotropy in solution. J Am Chem Soc 120:10947–10952

Garcia de la Torre J, Huertas ML, Carrasco B (2000) HYDRONMR: prediction of NMR relaxation of globular proteins from atomic-level structures and hydrodynamic calculations. J Magn Reson 147:138–146

Gaudin F, Paquet F, Chanteloup L, Beau JM, Thuong NT, Lancelot G (1995) Selectively C-13-enriched DNA-dynamics of the C1′–H1′ vector in D(CGCAAATTTGCG)(2). J Biomol NMR 5:49–58

Hall JB, Fushman D (2006) Variability of the ^{15}N chemical shielding tensors in the B3 domain of protein G from ^{15}N relaxation measurements at several fields. Implications for backbone order parameters. J Am Chem Soc 128:7855–7870

Hansen AL, Al-Hashimi HM (2006) Insight into the CSA tensors of nucleobase carbons in RNA polynucleotides from solution measurements of residual CSA: towards new long-range orientational constraints. J Magn Reson 179:299–307

Hansen AL, Nikolova EN, Casiano-Negroni A, Al-Hashimi HM (2009) Extending the range of microsecond-to-millisecond chemical exchange detected in labeled and unlabeled nucleic acids by selective carbon R(1rho) NMR spectroscopy. J Am Chem Soc 131:3818–3819

Hashim MA-H (2007) Beyond static structures of RNA by NMR: folding, refolding, and dynamics at atomic resolution. Biopolymers 86:345–347

Heisaburo S (1980) NMR relaxation processes of ^{31}P in macromolecules. Biopolymers 19:509–522

Hemminga MA, de Jager PA, Krüse J, Lamerichs RMJN (1987) Magic-angle-spinning NMR on solid biological systems. Analysis of the origin of the spectral linewidths. J Magn Reson 1969(71):446–460

Herzfeld J, Griffin RG, Haberkorn RA (1978) 31P chemical-shift tensors in barium diethyl phosphate and urea-phosphoric acid: model compounds for phospholipid head-group studies. Biochemistry 17:2711–2718

Heus HA, Wijmenga SS, van de Ven FJM, Hilbers CW (1994) Sequential backbone assignment in 13C-Labeled RNA via through-bond coherence transfer using three-dimensional triple resonance spectroscopy (1H, 13C, 31P) and two-dimensional hetero TOCSY. J Am Chem Soc 116:4983–4984

Hobartner C, Micura R (2003) Bistable secondary structures of small RNAs and their structural probing by comparative imino proton NMR spectroscopy. J Mol Biol 325:421–431

Hobartner C, Mittendorfer H, Breuker K, Micura R (2004) Triggering of RNA secondary structures by a functionalized nucleobase. Angew Chem Int Ed Engl 43:3922–3925

Hoogstraten CG, Wank JR, Pardi A (2000) Active site dynamics in the lead-dependent ribozyme. Biochemistry 39:9951–9958

Johnson JE, Hoogstraten CG (2008) Extensive backbone dynamics in the GCAA RNA tetraloop analyzed using (13)C NMR spin relaxation and specific isotope labeling. J Am Chem Soc 130:16757–16769

Johnson JE Jr, Julien KR, Hoogstraten CG (2006) Alternate-site isotopic labeling of ribonucleotides for NMR studies of ribose conformational dynamics in RNA. J Biomol NMR 35:261–274

Kan JH, Cremers AF, Haasnoot CA, Hilbers CW (1987) The dynamical structure of the RNA in alfalfa mosaic virus studied by 31P-nuclear magnetic resonance. Eur J Biochem 168:635–639

Kellogg GW (1992) Proton-detected hetero-TOCSY experiments with application to nucleic acids. J Magn Reson 1969(98):176–182

Kojima C, Ono A, Kainosho M, James TL (1998) DNA duplex dynamics: NMR relaxation studies of a decamer with uniformly 13C-labeled purine nucleotides. J Magn Reson 135:310–333

Koplin J, Mu Y, Richter C, Schwalbe H, Stock G (2005) Structure and dynamics of an RNA tetraloop: a joint molecular dynamics and NMR study. Structure 13:1255–1267

Kroenke CD, Rance M, Palmer AG (1999) Variability of the ^{15}N chemical shift anisotropy in *Escherichia coli* ribonuclease H in solution. J Am Chem Soc 121:10119–10125

Lane AN, Jenkins TC, Brown T, Neidle S (1991) Interaction of berenil with the EcoRI dodecamer d(CGCGAATTCGCG)2 in solution studied by NMR. Biochemistry 30:1372–1385

Lang K, Rieder R, Micura R (2007) Ligand-induced folding of the thiM TPP riboswitch investigated by a structure-based fluorescence spectroscopic approach. Nucleic Acids Res 35:5370–5378

Lipari G, Szabo A (1982a) Model-free approach to the interpretation of nuclear magnetic resonance relaxation in macromolecules. 1. Theory and range of validity. J Am Chem Soc 104:4546–4559

Lipari G, Szabo A (1982b) Model-free approach to the interpretation of nuclear magnetic resonance relaxation in macromolecules. 2. Analysis of experimental results. J Am Chem Soc 104:4559–4570

Loth K, Pelupessy P, Bodenhausen G (2005) Chemical shift anisotropy tensors of carbonyl, nitrogen, and amide proton nuclei in proteins through cross-correlated relaxation in NMR spectroscopy. J Am Chem Soc 127:6062–6068

Lynch SR, Puglisi JD (2001) Structure of a eukaryotic decoding region A-site RNA. J Mol Biol 306:1023–1035

Magusin PC, Hemminga MA (1993) A theoretical study of rotational diffusion models for rod-shaped viruses. The influence of motion on 31P nuclear magnetic resonance lineshapes and transversal relaxation. Biophys J 64:1851–1860

Magusin PC, Hemminga MA (1994) Analysis of 31P MAS NMR spectra and transversal relaxation of bacteriophage M13 and tobacco mosaic virus. Biophys J 66:1197–1208

Mandel AM, Akke M, Palmer IIIAG (1995) Backbone dynamics of *Escherichia coli* ribonuclease HI: correlations with structure and function in an active enzyme. J Mol Biol 246:144–163

Marino JP, Schwalbe H, Anklin C, Bermel W, Crothers DM, Griesinger C (1994) Three-dimensional triple-resonance 1H, 13C, 31P experiment: sequential through-bond correlation of ribose protons and intervening phosphorus along the RNA oligonucleotide backbone. J Am Chem Soc 116:6472–6473

Marino JP, Schwalbe H, Anklin C, Bermel W, Crothers DM, Griesinger C (1995) Sequential correlation of anomeric ribose protons and intervening phosphorus in RNA oligonucleotides by a 1H, 13C, 31P triple resonance experiment: HCP-CCH-TOCSY. J Biomol NMR 5:87–92

Miller JL, Kollman PA (1997) Theoretical studies of an exceptionally stable RNA tetraloop: observation of convergence from an incorrect NMR structure to the correct one using unrestrained molecular dynamics. J Mol Biol 270:436–450

Narberhaus F, Waldminghaus T, Chowdhury S (2006) RNA thermometers. FEMS Microbiol Rev 30:3–16

Nina M, Simonson T (2002) Molecular dynamics of the tRNAAla acceptor stem: comparison between continuum reaction field and particle-mesh Ewald electrostatic treatments. J Phys Chem B 106:3696–3705

Oberstrass FC, Allain FH, Ravindranathan S (2008) Changes in dynamics of SRE-RNA on binding to the VTS1p-SAM domain studied by 13C NMR relaxation. J Am Chem Soc 130:12007–12020

Odahara T, Nishimoto S, Katsutani N, Kyogoku Y, Morimoto Y, Matsushiro A, Akutsu H (1994) Dynamic properties of nucleic acids in biosupramolecular systems, as studied by 31P NMR. J Biochem 115:270–278

Olsen JI, Schweizer MP, Walkiw IJ, Hamill WD Jr, Horton WJ, Grant DM (1982) Carbon-13 NMR relaxation studies of pre-melt structural dynamics in [4–13C-uracil] labeled E. coli transfer RNAIVal. Nucleic Acids Res 10:4449–4464

Precechtelova J, Padrta P, Munzarova ML, Sklenar V (2008) 31P chemical shift tensors for canonical and non-canonical conformations of nucleic acids: a DFT study and NMR implications. J Phys Chem B 112:3470–3478

Reichert D, Pascui O, deAzevedo ER, Bonagamba TJ, Arnold K, Huster D (2004) A solid-state NMR study of the fast and slow dynamics of collagen fibrils at varying hydration levels. Magn Reson Chem 42:276–284

Rieder R, Lang K, Graber D, Micura R (2007) Ligand-induced folding of the adenosine deaminase A-riboswitch and implications on riboswitch translational control. Chembiochem 8:896–902

Schmidt PG, Playl T, Agris PF (1983) Internal dynamics of transfer ribonucleic acid determined by nuclear magnetic resonance of carbon-13-enriched ribose carbon 1. Biochemistry 22:1408–1415

Schmidt PG, Sierzputowska-Gracz H, Agris PF (1987) Internal motions in yeast phenylalanine transfer RNA from 13C NMR relaxation rates of modified base methyl groups: a model-free approach. Biochemistry 26:8529–8534

Schwalbe H, Buck J, Furtig B, Noeske J, Wohnert J (2007) Structures of RNA switches: insight into molecular recognition and tertiary structure. Angew Chem Int Ed Engl 46:1212–1219

Shajani Z, Varani G (2005) 13C NMR relaxation studies of RNA base and ribose nuclei reveal a complex pattern of motions in the RNA binding site for human U1A protein. J Mol Biol 349: 699–715

Shajani Z, Varani G (2007) NMR studies of dynamics in RNA and DNA by 13C relaxation. Biopolymers 86:348–359

Shajani Z, Drobny G, Varani G (2007) Binding of U1A protein changes RNA dynamics as observed by 13C NMR relaxation studies. Biochemistry 46:5875–5883

Showalter SA, Baker NA, Tang C, Hall KB (2005) Iron responsive element RNA flexibility described by NMR and isotropic reorientational eigenmode dynamics. J Biomol NMR 32:179–193

Spielmann HP (1998) Dynamics in psoralen-damaged DNA by 1H-detected natural abundance 13C NMR spectroscopy. Biochemistry 37:5426–5438

Terao T, Matsui S, Akasaka K (1977) Phosphorus-31 chemical shift anisotropy in solid nucleic acids. J Am Chem Soc 99:6136–6138

Tucker BJ, Breaker RR (2005) Riboswitches as versatile gene control elements. Curr Opin Struct Biol 15:342–348

Vallurupalli P, Kay LE (2005) A suite of 2H NMR spin relaxation experiments for the measurement of RNA dynamics. J Am Chem Soc 127:6893–6901

Varani G, Tinoco I Jr (1991) RNA structure and NMR spectroscopy. Q Rev Biophys 24:479–532

Villa A, Stock G (2006) What NMR relaxation can tell us about the internal motion of an RNA Hairpin: a molecular dynamics simulation study. J. Chem. Theory Comput. 2:1228–1236

Villa A, Widjajakusuma E, Stock G (2008) Molecular dynamics simulation of the structure, dynamics, and thermostability of the RNA hairpins uCACGg and cUUCGg. J Phys Chem B 112:134–142

Vokacova Z, Budesinsky M, Rosenberg I, Schneider B, Sponer J, Sychrovsky V (2009) Structure and dynamics of the ApA, ApC, CpA, and CpC RNA dinucleoside monophosphates resolved with NMR scalar spin–spin couplings. J Phys Chem B 113:1182–1191

Waldminghaus T, Heidrich N, Brantl S, Narberhaus F (2007) FourU: a novel type of RNA thermometer in *Salmonella*. Mol Microbiol 65:413–424

Wenter P, Fürtig B, Hainard A, Schwalbe H, Pitsch S (2005) Kinetics of photoinduced RNA refolding by real-time NMR spectroscopy. Angew Chem Int Ed Engl 44:2600–2603

Wenter P, Bodenhausen G, Dittmer J, Pitsch S (2006a) Kinetics of RNA refolding in dynamic equilibrium by ^{1}H-detected ^{15}N exchange NMR spectroscopy. J Am Chem Soc 128:7579–7587

Wenter P, Fürtig B, Hainard A, Schwalbe H, Pitsch S (2006b) A caged uridine for the selective preparation of an RNA fold and determination of its refolding kinetics by real-time NMR. Chembiochem 7:417–420

Williams DJ, Hall KB (1999) Unrestrained stochastic dynamics simulations of the UUCG tetraloop using an implicit solvation model. Biophys J 76:3192–3205

Williams DJ, Hall KB (2000) Experimental and theoretical studies of the effects of deoxyribose substitutions on the stability of the UUCG tetraloop. J Mol Biol 297:251–265

Williams DJ, Boots JL, Hall KB (2001) Thermodynamics of 2′-ribose substitutions in UUCG tetraloops. RNA 7:44–53

Williamson JR, Boxer SG (1989a) Multinuclear NMR studies of DNA hairpins. 1. Structure and dynamics of d(CGCGTTG TTCGCG). Biochemistry 28:2819–2831

Williamson JR, Boxer SG (1989b) Multinuclear NMR studies of DNA hairpins. 2. Sequence-dependent structural variations. Biochemistry 28:2831–2836

Winkler WC (2005) Riboswitches and the role of noncoding RNAs in bacterial metabolic control. Curr Opin Chem Biol 9:594–602

Zhang Q, Sun X, Watt ED, Al-Hashimi HM (2006) Resolving the motional modes that code for RNA adaptation. Science 311:653–656

Zhang Q, Stelzer AC, Fisher CK, Al-Hashimi HM (2007) Visualizing spatially correlated dynamics that directs RNA conformational transitions. Nature 450:1263–1267